J Mater Sci (2007) 42:6866–6877
DOI 10.1007/s10853-007-1502-4

Influence of thermal and mechanical surface modifications induced by laser shock processing on the initiation of corrosion pits in 316L stainless steel

Patrice Peyre · C. Carboni · P. Forget · G. Beranger · C. Lemaitre · D. Stuart

Received: 13 January 2006 / Accepted: 5 January 2007 / Published online: 30 April 2007

Abstract Pure mechanical and thermo-mechanical laser shock processing treatments have been carried out on an AISI 316L stainless steel. Surface properties, mostly mechanical and metallurgical modifications, were analysed at different scales: a local scale using the nano-indentation technique and AFM analysis, and a more macroscopic scale, using microhardness, optical microscopy and residual stress determinations. After a pure mechanical laser-peening treatment, a significant improvement in the pitting corrosion resistance (+0.1 V) was observed in 0.05 M NaCl. This improvement was attributed to the combined effects of compressive residual stresses and work-hardening, and, in turn, to a mechano-electrochemical phenomenon by which a modification of cathodic reactions occurs during electrochemical tests. For the surface treated by thermo-mechanical laser peening (combination of a surface ablation and shock waves), a tendency for decreasing resistance against pitting corrosion was shown, and attributed to the processing-specific surface texture (ablation craters), which made the material susceptible for the creation of occluded cells.

P. Peyre (✉) · C. Carboni · D. Stuart
GERAILP-LALP, UPR 1578 CNRS, 16bis Avenue Prieur de la Côte d'Or, 94114 Arcueil, France
e-mail: p.peyre@gerailp.fr

P. Forget
Cea-Saclay, 91191 Gif Sur Yvette, France

G. Beranger · C. Lemaitre
Laboratoire ROBERVAL, UTC, 60205 Compiegne Cedex, France

Introduction

Over the past 15 years, lasers have been widely envisaged for improving the electrochemical properties of stainless steel surfaces by creating surface alloys, or by rather simple surface meltings [1, 2], resulting in the modification of their resistance to pitting or intergranular corrosion and stress corrosion cracking. The conventional laser surface treatments are mainly thermal or thermo-chemical. Recently, new laser applications have emerged, called laser shock processing or laser peening, that allow surface properties to be modified by pure mechanical or thermo-mechanical effects. These novel applications are mostly directed to improving fatigue or wear properties [3], but also to the improvement of stress corrosion cracking behaviour, as shown recently by Sano et al. [4] on reactor vessels in Japanese power plants. The basic principle is rather simple: (1) a high energy—short duration laser pulse is focussed on a metallic target and creates a plasma, (2) this high temperature—high pressure plasma generates shock waves that deform the irradiated metal surface plastically and induce work-hardening and residual stresses. If the surface is insulated from the increasing thermal gradient by a protective overlay (adhesive or paint), the laser treatment becomes purely mechanical. When the shock wave generation occurs together with surface ablation and melting (without a protective overlay), the treatment becomes thermo-mechanical and the affected depths are in the 5–50 μm range. In that case, thermal loading of the surface involves up to 20,000 K peak temperature during a few μs (a much longer time than the shock wave duration due to plasma confining effects). Thus, for industrial applications, the use of either pure mechanical, or thermo-mechanical laser treatments can be challenging yet beneficial, not only for mechanical resistance, but also

for corrosion properties, and especially pitting corrosion which is usually considered to be a precursor to corrosion fatigue or stress corrosion cracking in chloride solutions. In this context, the purpose of this paper is to report on the results of experiments describing the improvement of the corrosion properties of laser treated surfaces, in thermo-mechanical or pure mechanical conditions. In addition, following previous research on the same steel [5] that had received only pure mechanical treatments and was subsequently tested in a corrosive environment with a higher chloride content, our goal was two-fold:

(i) to compare chemical, microstructural and mechanical surface modifications induced by pure mechanical or thermo-mechanical laser surface treatments; and
(ii) to explore how these surface states may influence corrosion pit initiation in type 316L stainless steels.

Numerous investigations [6–8] have been performed in which the influence of a surface residual mechanical stress field on the physicochemical properties such as passivation or pit initiation have been reported, without giving any precise explanation about the modifications observed. This work attempts to provide such an explanation.

Experimental

Material

Experiments were performed on a type 316L stainless steel provided by Creusot-Loire Industries in the form of 13 mm thick laminated plates, in a as-quenched metallurgical state (1,060 °C for 2 h, followed by water quenching), with a distribution of generally equiaxed grain (30–70 μm γ grain sizes). The 0.2% yield and ultimate tensile strengths of the steel (noted by $R_{P0.2}$ and R_m) are 310 MPa and 400 MPa, respectively. The chemical content (determined by Glow Discharge Optical Spectroscopy (GDOS)) exhibits (Table 1) a 0.019 wt% carbon content and a low sulfur content (0.007 wt%) to limit the formation of MnS inclusions, which are known to be harmful for the pitting corrosion resistance [9]. Semi-quantitative EDX analysis indicated that the non-metallic inclusions present in the steel were primarily in the form of binary or ternary oxide aggregates with Al, Si, Ti, Mg, Mn and Ca as main elements. The density of these inclusions was estimated to nearly 30 inclusions/mm^2. The same steel had been characterized and used in previous publications [5, 10, 11].

Table 1 Composition (weight %) of AISI 316L stainless steel [5]

Element	C	Mn	S	Si	Ni	Cr	Mo	Fe
Content (wt%)	0.019	1.68	0.007	0.35	11.95	17.1	2.0	Balance

Basics of the laser experiments and experimental conditions

Developed in the early 70s in the USA [3], the laser shock processing or laser-peening treatment is only emerging now as a serious candidate for locally hardening surfaces and improving material properties by imparting compressive residual stresses to the surface. The basics of the process are summarized in Fig. 1.

During thermo-mechanical laser peening, heat propagation due to the temperature rise of the plasma (between 10,000 K and 20,000 K) follows shock wave propagation induced by the plasma expansion. The resulting effects are expected to be the occurrence of surface ablation (1–2 μm) and melting, combined with the laser-induced shock compression.

When using a protective overlay, heat propagation does not affect the metal target, which is only submitted to shock waves. Resulting effects are purely mechanical, just like a conventional shot-peening. Usually, a laser peening (LP) treatment is carried out in a water-confined regime (the target is immersed in water) to increase the plasma pressure by a trapping-like effect on the plasma expansion [12]. In the 3–6 ns pulse duration regime, the plasma pressure follows a $P(\text{GPa}) \approx 1.6\sqrt{I(\text{GW/cm}^2)}$ empirical relationship [10], with 7–8 GPa maximum pressure values. Both configurations (with or without coatings) have industrial applications in the field of fatigue or stress corrosion cracking [4] of nuclear components. However, a comparison of surface states generated by both treatments has never been presented.

Laser-peening (LP) conditions have been selected such that surfaces are submitted to either mechanical or combined thermal + mechanical treatment:

– The first experiments were carried out with the Nd: Glass laser from LULI laboratory,[1] operating at 1.06 μm and delivering 80 J in 3 ns pulses. The 13 mm impacts have been used with a laser intensity of 20 GW/cm^2, resulting in a 7–8 GPa maximum pressure. A 60–70 μm protective coating (Aluminium paint) was used to ensure a pure mechanical treatment. Three or six local impacts were used.
– The thermo-mechanical surface treatment was carried out at the University of Göettingen (Germany), with the same laser conditions as those used in Japan for the LP treatment of nuclear plants components [13]. In this case, 1 mm impacts were used, at 6 GW/cm^2 laser intensity (estimated pressure = 4 GPa), with a high coverage rate resulting in about 38 local impacts. Moreover, the laser wavelength was 0.532 μm, i.e., the first harmonic of 1.06 μm Nd: YAG wavelength.

[1] Laboratoire pour l'Utilisation des Lasers Intenses, UMR 7605 CNRS, 91128 Palaiseau cedex, France.

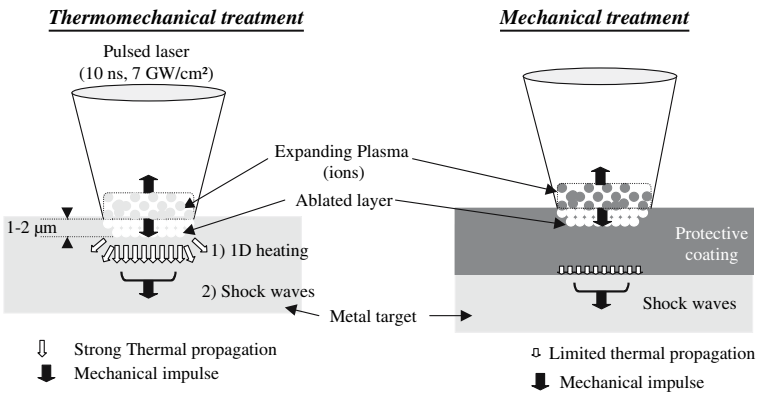

Fig. 1 Basic scheme of a mechanical or thermo-mechanical laser-peening treatment

The details for both treatments are presented in Fig. 2. These treatments were applied to 14 mm diameter cylinders for corrosion tests. The experimental conditions are summarized in Table 2.

Experimental characterization of surface modifications

Microstructural and chemical analysis

The samples studied were 14 mm in diameter, 8 mm in height cylinders cut by electro-discharge machining. Prior to laser treatment, the cylinders were mechanically polished with silicon carbide emery papers down to 2,400 grit, polished with a SiO_2 suspension down to 0.03 µm average roughness, then ultrasonically rinsed in ethanol.

Different techniques were used to characterize the surface condition after laser treatments, including geometrical, metallurgical, chemical and mechanical analysis of the surface layers.

Geometrical changes were analysed with a 1D profilometer (Perthometer) with a 0.2 mm/s stylus displacement to determine the average and maximum roughness and waviness values over a linear distance of 5 mm.

Optical microscopy was performed on the top surfaces as well as cross sections between 100× and 400× magni-

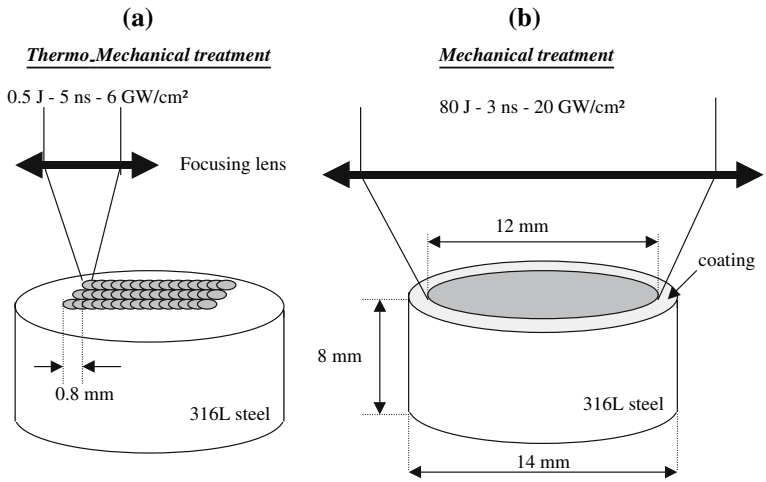

Fig. 2 Experimental conditions for LP treatments: (**a**) Thermo-mechanical treatment with 0.8 mm laser impacts, (**b**) mechanical treatment with 12 mm impacts

Table 2 Experimental laser conditions

	Wavelength (µm)	Pulse duration τ (ns)	Energy per pulse (J)	Impact diameter (mm)	Laser intensity (GW/cm^2)	Number of local impacts
Thermo-mechanical treatment	0.53	5	0.5	0.8	6	38
Mechanical treatment	1.06	3	80	12	20	3

fications to analyse the deformation structure. Also, atomic force microscopy allowed us to identify more precisely the surface topography after LP.

Specimen characterization using scanning electron microscopy (using a JEOL 6300 scanning electron microscope) coupled with energy dispersive X-ray spectrometry (EDX), and electron probe microanalysis (EPMA) (using a Cameca SX50 at 15 kV) was also performed to analyse inclusions, and inclusion–matrix interfaces after LP.

Secondary Ion Mass Spectroscopy (SIMS) analysis was also performed using a primary Ar^+ ion incident beam (200 nA–12.5 kV) with a 60 μm probe diameter. This enabled us to determine in-depth compositional fluctuations where O, Cr, Ni, Mo and Al elements were analysed.

Mechanical analysis

Mechanical modifications induced by laser peening were analysed using microhardness measurements, nano-indentation tests, and residual stress determinations with the X-ray diffraction technique.

Microhardness tests were carried out using a Vickers indentor under a 50 N load on as-polished and laser-peened specimens. For each surface condition, an average microhardness value has been determined, based on a minimum of 10 indentations. The average depth of indentation was nearly 10 μm.

Nano-indentation tests have been performed with a pyramidal Berkovich diamond indentor (E_i = 1,141 GPa). For the thermo-mechanical sample, tests were carried out after removing approximately 10 μm by surface polishing (on the mechanically affected zone below the ablated layer) due to the high roughness that prevented a precise determination of the indented areas. In the loading direction, the depth of indentation ''h'' increased up to maximum load value. Then, in the unloading direction, h decreased with decreasing load, down to the residual plastic indentation value (typically 80 nm to 0.28 μm in our case).

Figure 9 shows typical load–depth curves F = f(h) at various maximum loads (1 mN, 3 mN, 10 mN), on as-polished and laser-peening samples with or without thermal ablation. These load–depth curves were obtained by averaging 10–20 load–depth curves for each surface condition. The mechanical properties such as hardness H and elastic modulus E can be evaluated from the curves F = f(h).

First, the hardness was obtained by dividing the maximum load F_{max} by the projected contact area A, where A can be estimated from the actual indentation depth h_c at the maximum load ($A \approx 2.6\, h_c^2$) [14]. Second, the Young modulus of the metal E_m was determined from the slope of F = f(h) curves (Eq. 1), and the elastic properties of the diamond indentor (E_i and ν_i).

$$\frac{dF}{dh} = \beta \cdot E^* \cdot \sqrt{A} \tag{1}$$

with A = projected contact area of the indentation, $\beta = 2/\sqrt{\pi}$ for a Berkovich indentor and E^* = reduced modulus with $\frac{1}{E^*} = \frac{1-\nu_i^2}{E_i^2} + \frac{1-\nu_m^2}{E_m^2}$.

X-ray diffraction was used as a residual stress determination method, with the use of the classical $2\Theta = f(\sin^2\psi)$ method [15]. Experimental conditions were: a Mn anticathode with a Cr filter, Bragg angle = 152°, 13 Ψ angles and 1 ϕ angle. For these experimental conditions, the penetration depth of X-rays is about 5–10 μm in stainless steels. Surface and in-depth analysis (with electropolishing matter removal) allowed us to determine the thickness of thermally and mechanically affected layers.

Electrochemical experiments

A three electrode device was used for our corrosion tests: including a 14 mm diameter platinum disk and a Hg/Hg_2Cl_2 (SCE) as counter and reference electrodes, respectively, and the metal surface as work electrode. A Solartron 1184 electrochemical interface was used to control the experiments.

The following electrochemical experiments were carried out in 0.05 M NaCl solution, after 5 min immersion of the samples in an ultrasonic cleaning system:

(i) open circuit potential measurements E = f(t) to determine rest potentials E_{rest},
(ii) potentio-dynamic tests I = f(E) at 2 mV/s scanning rate, starting from –0.6 V/SCE cathodic value up to the pit initiation potential E_{GP}, followed by a potential scan reversal above an intensity threshold of 200 $\mu A/cm^2$ to determine the protection (or repassivating) potential E_{PP}. Stable pitting is recognizable by a sharp current density increase, where E_{GP} is considered at 10 $\mu A/cm^2$. Such dynamically determined potentials are, in relation with stationary pitting potentials, always shifted to nobler values.

The potentio-dynamic tests were started after a 30 s cathodic polarization at –0.6 V/SCE potential in order to depassivate the surface and/or to start experiments from a similar passive surface state. For each surface condition, at least 3–4 corrosion tests were performed in 0.05 M NaCl—pH 6.7 solution, with a normalized cell (CKE230 cell) and a constant electrolyte flow in the cell.

Surface modifications induced by laser shock processing treatment

Surface aspects

Corrosion samples after mechanical (M) or thermo-mechanical (TM) treatments are presented in Fig. 3. After a pure mechanical treatment, surfaces are mostly preserved due to the good homogeneity of the laser source, and to the short pulse durations that create very short deformations. This is confirmed by the roughness measurements where average roughness values (R_a = 0.05 μm) were modified to a minimal extent as compared with the untreated metal (R_a = 0.03 μm).

The TM laser treatment generated a black opaque surface layer, with significant surface roughening due to the formation of ablation craters from the small (D = 0.8 mm) laser impacts, striking directly the metal surface. Thus, the resulting average roughness (R_a = 0.6 μm) is increased by a factor 30.

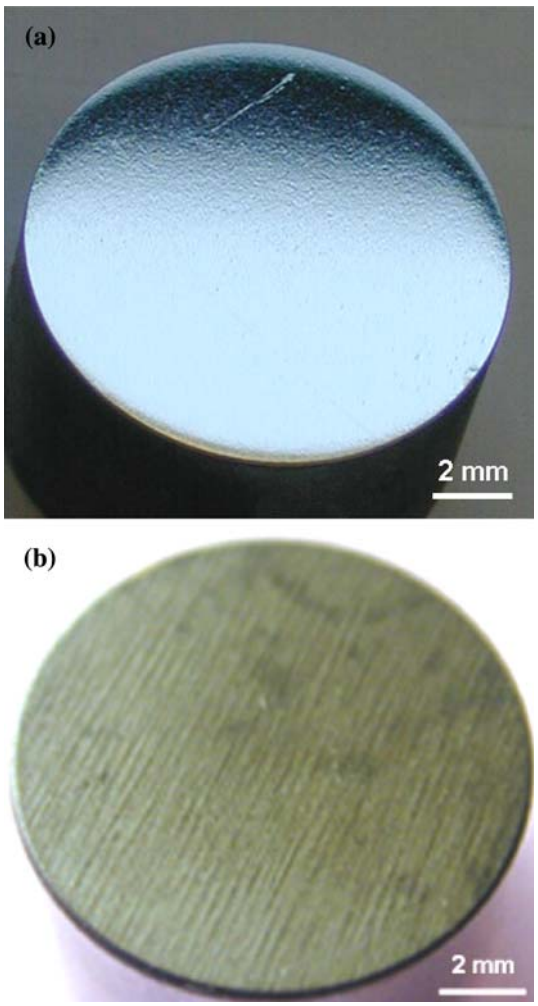

Fig. 3 Fourteen millimetre diameter corrosion samples treated by: (**a**) pure mechanical laser peening (the surface keeps a very reflective and smooth aspect), (**b**) thermo-mechanical laser peening (surface exhibits a striated and brown aspect due to impact overlapping and oxide formation)

Surface analysis with Secondary Ion Mass Spectroscopy (SIMS) and EDX spectrometry

Due to the pressure or temperature loadings submitted to metal surfaces, laser peening is expected to degrade and modify the surface chemistry because of impurity implantation effects or thermo-chemical diffusion.

On the one hand, after the mechanical LP treatment, the surface composition is kept nearly constant, indicating that no contamination has occurred (Fig. 4). This confirms that

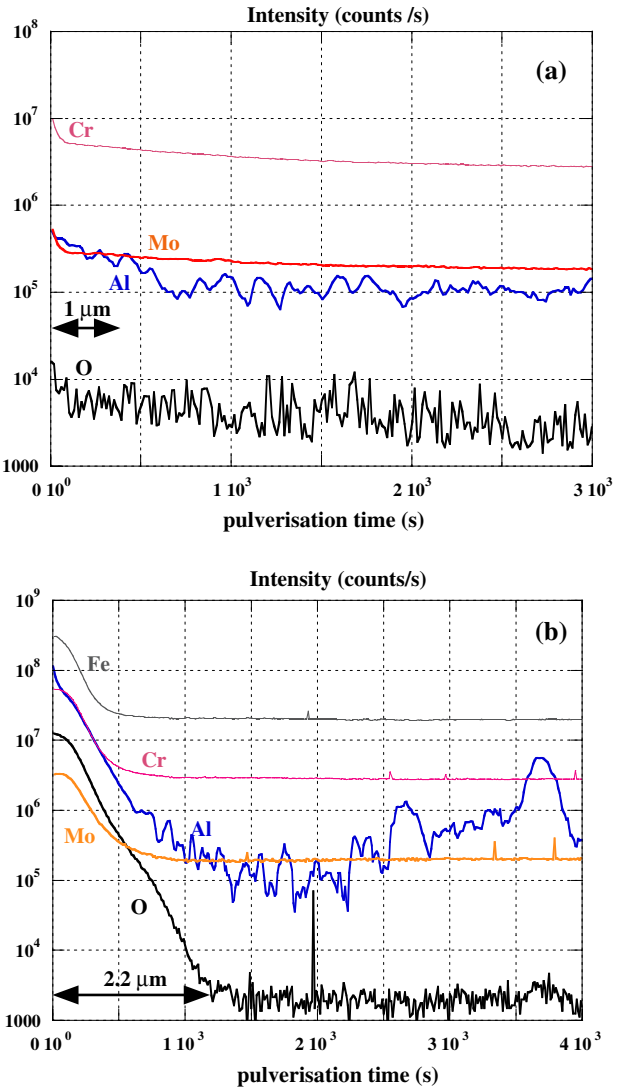

Fig. 4 SIMS profiles on laser treated surfaces: (**a**) pure mechanical laser peening, (**b**) thermo-mechanical laser peening. An enrichment with O, Al and Cr is evidenced on the first 2.2 μm in-depth after thermo-mechanical treatment

the protective coating has played its role, and that the surface was only submitted to a mechanical loading. On the other hand, the thermo-mechanical LP has modified the oxygen, aluminum and chromium profiles to a 2 μm depth (Fig. 4), indicating the presence of an oxide layer, corresponding to the opaque surface aspect shown in Fig. 3. Up to now, we do not have any explanation for the presence of aluminum in this layer (the base steel only contains low levels of Al).

Moreover, SEM EDX microanalysis carried out on 50 μm × 50 μm regions surrounding multi-element inclusions before and after LP, did not reveal any microstructural changes near the inclusion–matrix interfaces, or any inclusion removal due to shock wave effects.

Microstructure and surface topography

For the thermo-mechanical (TM) condition, the combination of ablation and melting of surface layers under water confinement produces a 2–3 μm residual oxide layer (Fig. 5). This layer is mainly chromium oxide. This oxide follows the micro-craterization of the surface (Fig. 6a, b), which provokes higher roughness values.

Below the thermally affected zone (after the removal of 5 μm by polishing), a severely deformed structure can be seen (Fig. 7b) due to the large number of impacts (38) that produce cyclic hardening. Numerous planar slip bands are shown in each γ grain, with 1 or 2 active slip systems. On the other hand, cross-sections do not show evidence of a melted layer (e.g., a very fine cellular or dendritic solidification structure) below the oxide layer of thermo-mechanical samples.

Laser peening in pure mechanical conditions (with the protective coating) usually produces planar slip bands in

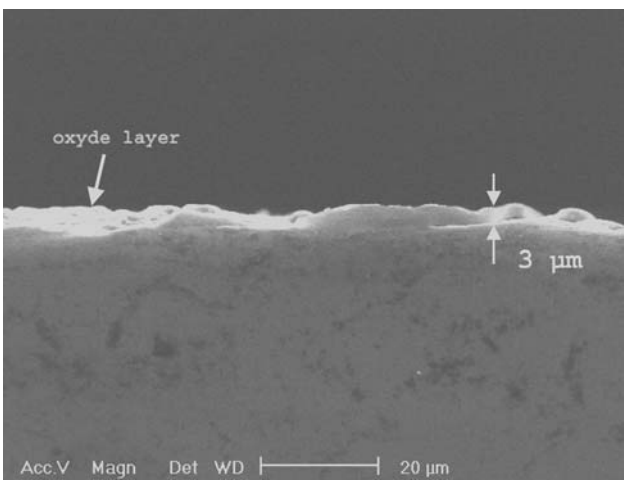

Fig. 5 Secondary electron micrograph showing the presence of a 3 μm thick oxide layer enriched with Cr on thermo-mechanical surface (as determined from EDX analysis)

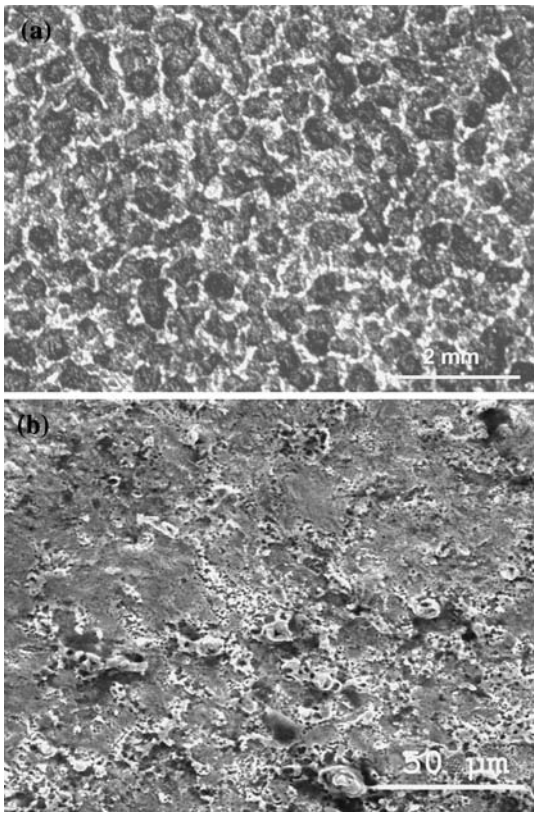

Fig. 6 Images of the surface after thermo-mechanical treatment: (**a**) optical micrograph showing ablation craters (nearly 0.5 mm diameter) on the oxidized layer, (**b**) SEM image at higher magnification revealing micro-holes on the treated surface

austenitic stainless steel, as reported in many investigations [5, 10, 11]. Figure 7a exhibits a classical deformation structure obtained after a 20 GW/cm^2—three impacts laser treatment. The observation that only one slip system seems to be activated in each γ grain ((110) direction in {111} planes) will be related to the orientation of the grains. Previous work has shown that the deformation structure may become more severe with more impact loadings [10].

Atomic Force Microscopy, performed within a few γ grains after LP treatment allowed us to characterize the topography of treated surfaces, and to measure the height of planar slip band emergence. For a limited number of planar slip bands and a large inter-planar slip band distance (>5 μm), the height of emergences is nearly 40–50 nm (mechanical LP: Fig. 8). These planar slip band amplitudes tended to decrease with the severity of treatment: more planar slip bands were present in each γ grain and the inter-slip band distance was shortened, but the height of emergence decreased to 20 nm values. These results indicated a rather inhomogeneous surface micro-roughening (dependent on the orientation of each γ grain versus the shock wave propagation axis), which could enhance pit initiation, and prevent the formation of an ideal passive layer (see Fig. 9).

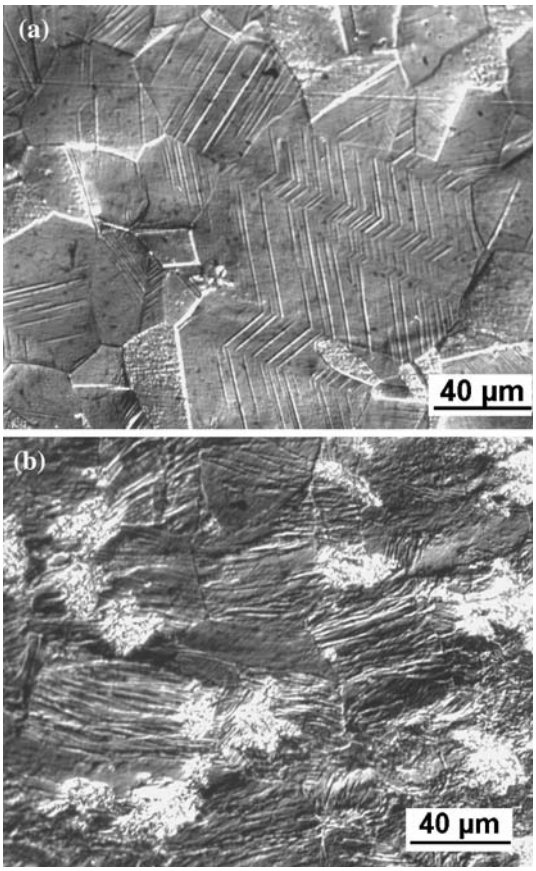

Fig. 7 Microstructures of laser-peened surfaces: (**a**) pure mechanical treatment: generation of planar slip bands in γ(grains (1 activated systems per grain), (**b**) thermo-mechanical treatment revealing 2–3 activated systems per grain (the surface oxide layer (bright) was partially removed by 4,000 SiC polishing to reveal the underlying deformation structure)

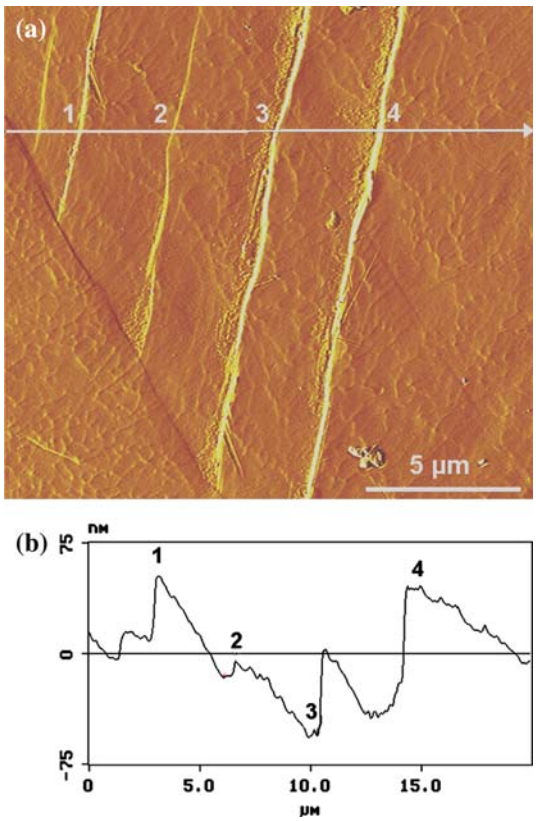

Fig. 8 AFM analysis of a laser-peened surface in pure mechanical condition: (**a**) surface aspect, (**b**) height versus distance profile which evidences the emergence of planar slip bands (inter-band distance = 2–3 µm, height of emergence = 50 ± 10 nm)

Mechanical modifications

Microhardness measurements and nano-indentation tests

We have reported in Fig. 10 the hardness values obtained after microhardness and nano-indentation tests under 3 mN load. Different values are obtained with the two techniques, but for each test, we can estimate the effects of a laser peening.

On the one hand, the microhardness tests reveal a small work-hardening effect on the surface, with a +10% hardness increase after laser peening (with or without thermal effects).

On the other hand, the nano-indentation tests indicate a –20% decrease of the surface hardness, when compared with the as-polished sample. These behaviours can be attributed to the work-hardening level before LP, which seems to be very severe on the first layers below the surface, due to a grinding effect, and much less severe 10 µm below. The thermo-mechanically treated surface is always

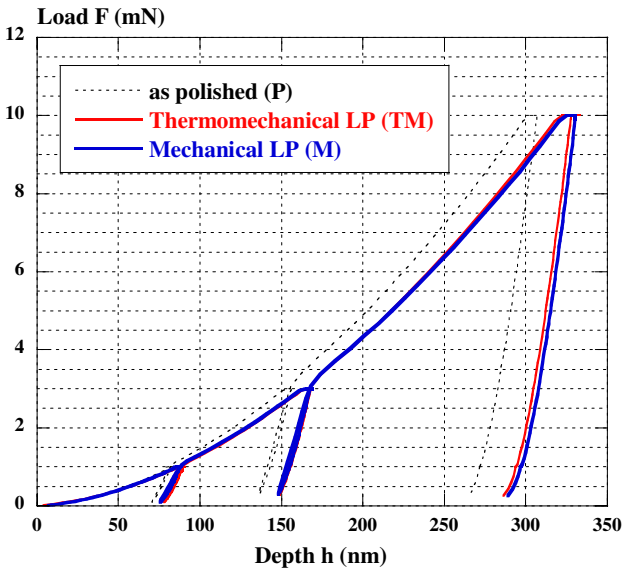

Fig. 9 Average load–depth nano-indentation curves for as-polished (P), mechanical LP (M) and thermo-mechanical LP (TM) surface conditions (averaged from 20 F = f(h) measurements). Three loads are applied: 1 mN, 3 mN and 10 mN

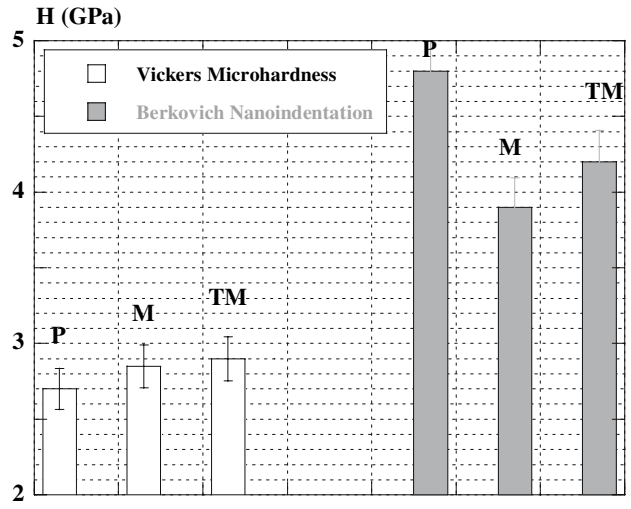

Fig. 10 Hardness determinations with microhardness and nano-indentation tests on as-polished (P), mechanical laser peening (M) and thermo-mechanical laser peening (TM). Nano and micro measurements provide opposite results concerning surface hardenings

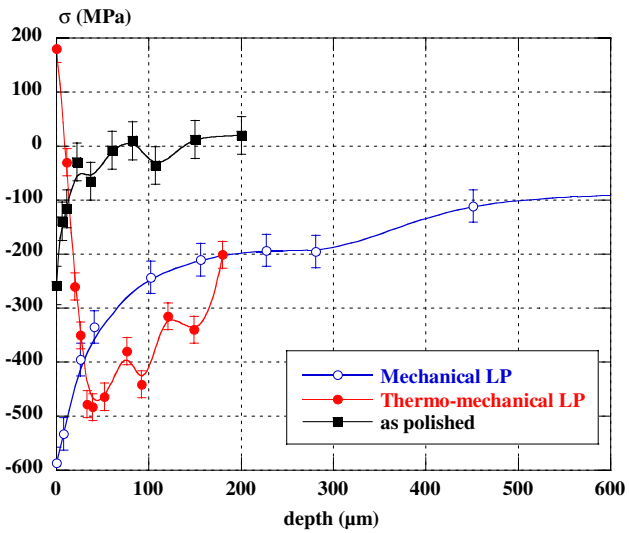

Fig. 11 In-depth residual stress determinations using X-ray diffraction technique on: (■) as-polished, (○) as-polished + mechanical LP and, (•) as-polished + thermo-mechanical LP. The thermo-mechanical treatment generates a strong tensile to compressive surface stress gradient on the first 20 μm in-depth

a little harder than the pure mechanical condition, because of a higher number of deformations that favours cyclic hardening on 316L stainless steel. If we now compare hardening effects estimated at a micro-scale or a nano-scale between (1) as-polished samples and (2) thermo-mechanical (TM) samples + 10 μm matter removal, we can assume that softening effects evidenced at a nano-scale after 10 μm matter removal should be underestimated, when compared with the very surface hardness. Indeed, shock pressure gradient is very small over the first 10 μm of impacted depths, whereas temperature gradient is extremely high. Consequently, if nano-indentation tests had been carried out on the very surface, even higher thermally induced softening would have been expectable.

Young modulus values have not been modified by surface treatments. Nano-indentation tests indicate constant values of about 210 ± 5 GPa on as-polished and LP specimens. These values are a little higher than those from macroscopic tensile or compressive tests (195 GPa).

Residual stress determinations

After a pure mechanical laser peening, the surface is under compressive stress, with maximum values close to –580 MPa, due to the heterogeneous surface deformation, and a cyclic hardening behaviour of 316L, which increases the elastic limit for a given strain amplitude (Fig. 11). This result is consistent with usual mechanical effects induced by LP on 316L steel [10].

On the thermo-mechanical (TM) sample, the combination of thermal (ablation + melting) and mechanical (shock waves) effects, generates tensile residual stresses on the first 10–20 μm (thermal effect), and a compressive stress field below. Thus, a very important stress gradient is evidenced on the first 30 μm, starting from a +180 MPa maximum surface stress, to a –480 MPa level at 30 μm below the surface. Thus, both laser-peening conditions (M and TM) can induce a large range of residual surface stress fields.

Electrochemical results

Rest potential versus time curves are shown in Fig. 12a and b, for a maximum recording time of 2 h. For all conditions, E_{rest} increased with time, due to the passive film growth. After a pure mechanical LP treatment (M), E_{rest} values were kept nearly equal to the base material values. On the other hand, a clear anodic ennoblement was evidenced on thermo-mechanically (TM) treated surface, but large potential fluctuations were shown (Fig. 12b), which may be due to the surface roughening and the presence of ablation craters that create possible occluded cells (de-aerated zones) and local galvanic coupling (due to strong plasticity gradients). In the TM case, the passive films grew on the pre-formed surface oxide (see Fig. 5). This could explain the higher E_{rest} values compared with those for the pure mechanical LP.

On mechanically treated (M) samples, a small (+20 mV) anodic shift was evidenced on all the specimens investigated so far, due to pure mechanical modifications. This result agrees with previous work on 316L stainless steel,

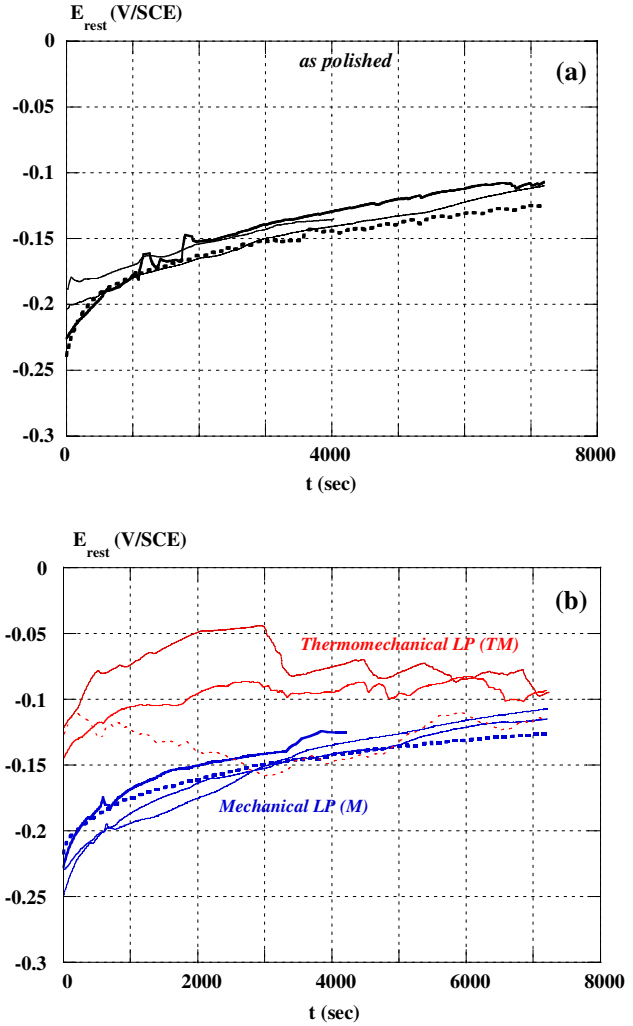

Fig. 12 Rest potential versus time recordings (open circuit conditions) for: (**a**) as-polished samples, (**b**) mechanical laser-peening (M) samples and thermo-mechanical (TM) samples

indicating an ennoblement after mechanical laser treatment [5, 10].

Potentio-kinetic curves I = f(E) are presented in Fig. 13a, b and c. For each surface condition, 4–5 experiments were carried out (only three are presented in Fig. 13 to simplify the demonstration). Mechanical or thermo-mechanical laser-peening procedures were shown to generate opposite effects:

(i) the thermo-mechanical (TM) treatment reduced E_{GP} and E_{PP} values (nearly –0.17 V/SCE), but also decreased the passive current density I_P by a factor 2 (5 μA/cm^2 to 2 μA/cm^2 average value at 0.1 V/SCE). This result seems to indicate a better passive film growth or a pre-established stable oxide layer.

(ii) The mechanical (M) treatment increased both E_{GP} and E_{PP} (by nearly +0.1 V/SCE) and generated a small I_P decrease (–0.5 μA/cm^2) compared with the as-polished sample. Thus, M samples with a high compressive stress level have the most pronounced passive area.

(iii) No real modification of the corrosion potential could be evidenced after both LP treatments (E_{corr} remains equal to –0.3 ± 0.02 V/SCE).

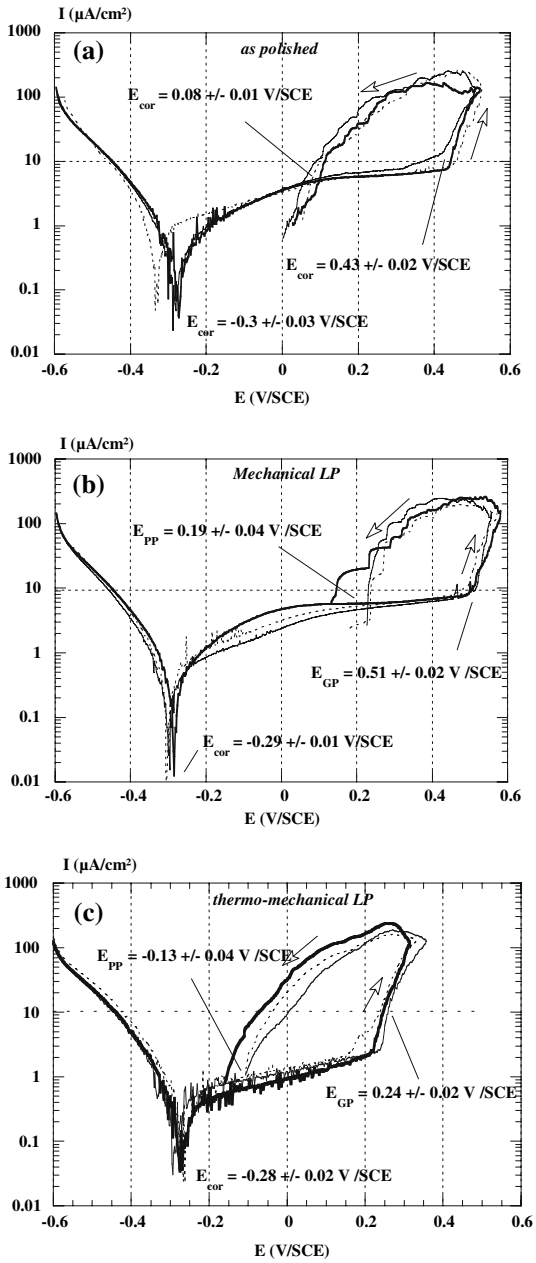

Fig. 13 Potentio-kinetic curves in NaCl 0.05 M at 2 mV/s scan rate for: (**a**) as-polished, (**b**) mechanical LP (M) and, (**c**) thermo-mechanical (TM) LP conditions (potential start at –0.6 V/SCE, current density threshold for potential scan reversal = 200 μA/cm^2). Three curves are presented for each condition

All these results are reproducible, as shown on Fig. 13a, b and c on as-polished, mechanical (M) and thermo-mechanical (TM) specimens.

Thus, pure mechanical modifications (compressive residual stresses) have a beneficial effect on pit initiation whereas thermo-mechanical effects (surface roughening + tensile residual stresses) cause early pitting, despite the generation of nobler surfaces.

Moreover, if we calculate the dissolved weight of metal with the use of Faraday's Law (Eq. 3),

$$m = \frac{S \cdot M_{Fe}}{2 \cdot \Im} \int_{t_1}^{t_2} I \cdot dt \quad (3)$$

with m = dissolved weight (g), $\Im$ = Faraday number (=96500 C), S = active area (m^2), I = current density (A/m^2), M_{Fe} = Molar weight (55.8 g for Iron).

We find values of 6.5 ± 1 µg before treatment, 5.7 ± 1 µg after mechanical peening and 4.5 ± 1 µg after thermo-mechanical peening. The reduction of weight losses becomes even more pronounced with a higher work-hardening level (after, for instance, a shot-peening treatment), in the same range of potentials. This appears to indicate a correlation between anodic dissolution (pit propagation), and the work-hardening level. This is confirmed by the analysis of pit depths: even though circular pit shapes are not modified, 20–25 µm average propagation was observed on as-polished samples versus 15–20 µm after mechanical LP and 12–14 µm average value on thermo-mechanical samples.

Analysis of pits

The pit shape is mostly circular (Fig. 14a), with diameters in the 10–50 µm range, without significant modifications in the number of pits after LP treatment (Fig. 15).

After LP, the corrosion pits seem to be localized mainly in the strongly deformed regions of the surface, i.e. those with a high planar slip bands density (Fig. 14b). Hence, a correlation between the pits density and the lattice distortion may be possible. However, their diameter and the global inclusion density (calculated from the whole sample surface), remained constant compared with the as-polished condition. Moreover, no occluded pits are observed as compared with other experiments carried out after LP on the same steel in acid chloride medium (pH = 1) [11].

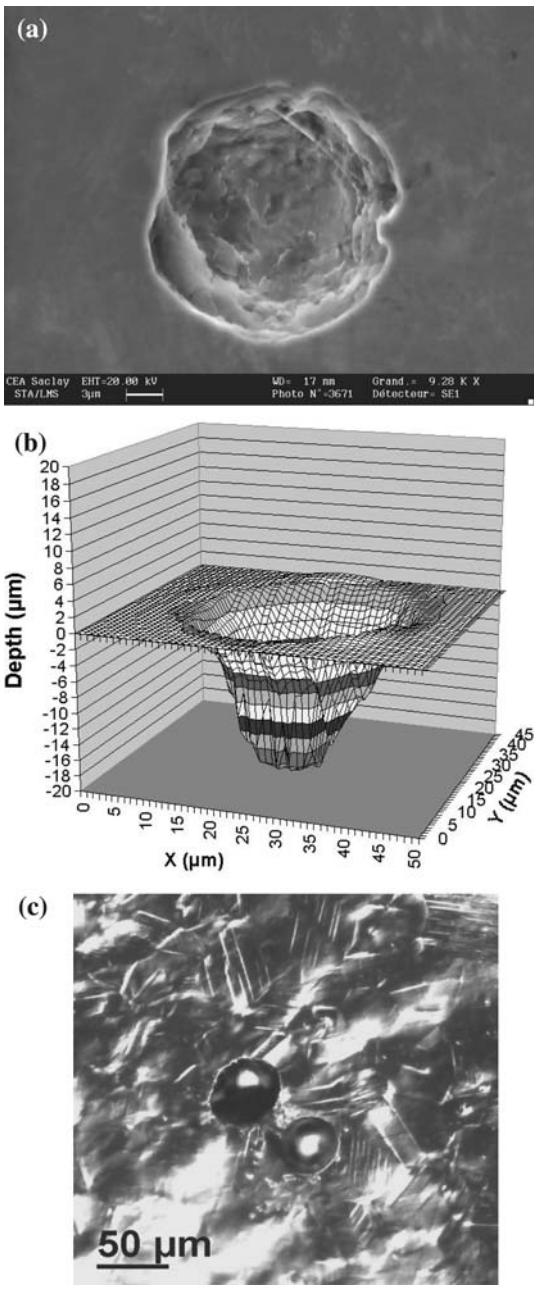

Fig. 14 Corrosion pits after a mechanical LP treatment: (**a**) detail of a circular pit, (**b**) 3D profile of the pit, (**c**) pits on a severely deformed area

Discussion

We have shown that the interaction of a high intensity (GW/cm^2) laser pulse could modify the pitting corrosion susceptibility of a stainless steel surface. Two ways have been explored: a thermo-mechanical laser peening (TM) and a pure mechanical configuration (M). Different For the TM samples, thermal effects (ablation and melting of surface layers) have been shown to create surface roughening that appeared to promote anticipated pit initiations on harmful inclusions (possibly those localized in craters). Another explanation could be a selective ablation of matrix surrounding inclusions, provoking critical zones in the near-inclusion regions. In that case, the lower corrosion resistance was clearly attributed to the surface topography change, and may be promoted by the tensile stress field.

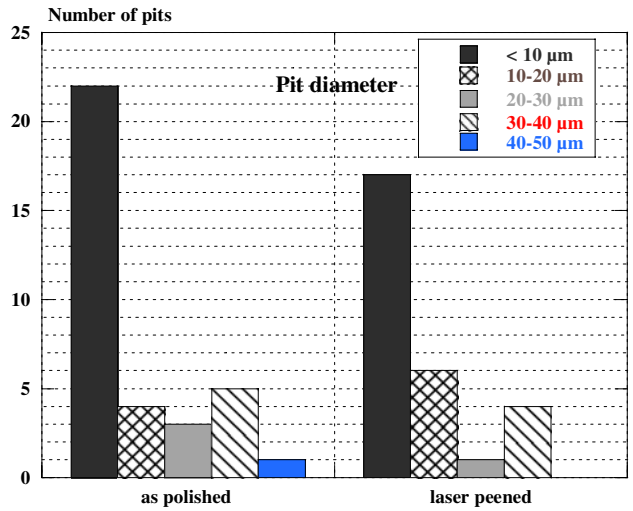

Fig. 15 Number of pits versus pit diameter on as-polished and laser-peened (M) specimens

The beneficial influence of a pure mechanical laser peening was not very obvious to understand: without any detectable composition change, a work-hardened surface was shown to become more noble and more resistant to pit initiation, despite small topography changes evidenced at a macro- and micro-scale. This is somewhat contradictory with conventional thinking, where nobler rest potentials exhibit smoother surfaces corresponding to defect-free passive layers. That kind of effect, whereby a mechanical state affects surface reactivity, has been reported by Ben Rhouma [8] and widely investigated by Gutman [16]. For instance, according to mechano-chemical theory, an increase in the hydrostatic pressure tends to provoke an activation of anodic dissolution (Formula 4).

$$I = i_a \cdot \exp\left(\frac{\sigma_m \cdot V_m}{RT}\right) - i_c \quad (4)$$

with V_m = molar volume, i_a = anodic current density, i_c = cathodic current density, I = global current density, σ_m = hydrostatic stress.

Moreover, it has been shown that, under static loading, a 304 stainless steel becomes less and less passive when submitted to increasing work-hardening levels [16].

In our case, characterization of the surface work-hardening does not provide the same information if carried out at the nano-scale (a softening is evidenced after both LP processes) or at a microscale (hardening is observed). This reveals the overall complexity of trying to correlate a surface-near mechanical state (work-hardening or residual stresses) to the electrochemical reactivity. One thing is certain: a mechanical surface state modifies the corrosion reactivity. In our case, despite a roughness increase (at a macroscale: R_a increases, and at a microscale: 20–50 nm planar slip band emergence is shown), a mechanical LP improves the pitting corrosion resistance. This is contradictory with the fact that, if we consider the deformation microstructure at a microscale, the generation of planar slip bands is expected to create local cathodic potential drops, and to increase the surface heterogeneity (Fig. 16).

The influence of residual stresses on the pitting corrosion susceptibility has not been reported to date, except in [6] after shot-peening or grinding treatments, or after laser peening type 304 stainless steel [13]. The experimental results differ: some indicate a negative influence of stresses (whatever the sign) on the corrosion reactivity [6]. Other publications indicate a possible beneficial effect of compressive surface stress fields [5].

Therefore, it is only possible to speculate on the reasons for our results:

(i) The small ennoblement generated after LP reduces the potential gap between non-metallic inclusions (at high potential) and the surrounding matrix. This results in a reduction of local galvanic couplings and, possibly, a reduction of pit initiation sensitivity.

(ii) The passive film grown on a surface with a high compressive stress field has been previously shown to be thinner [10], but possibly more compact and more resistant to breakdown when subjected to electrostrictive stresses. This cathodic origin of the mechano-chemical modifications seems to be more likely to occur as many investigations on other passive materials (high Cr stainless steels) showed important modifications in the cathodic part of potentio-kinetic curves, such as a severe decrease of cathodic current.

To confirm these assumptions, a local electrochemical approaches could be employed to provide useful information, such as scanning vibratory electrode techniques (SVET) or micro-electrochemical cells [17] to analyse electrochemical gradients between severely deformed and non-deformed areas, or between inclusions and matrix. The

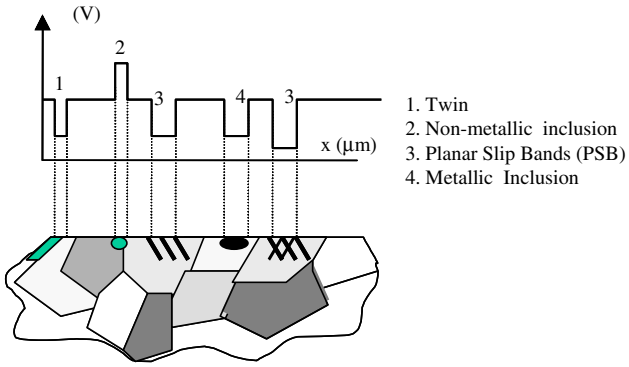

Fig. 16 Local potential versus distance on a deformed microstructure (from [16])

use of the nano-indentation technique might also be a useful novel method to characterize mechanical properties of the passive film itself, with very low applied stresses and indentation depths (around 10 nm as reported in [18]).

Lastly, it appears that very severe work-hardening and residual stress levels could reduce the pit propagation. This result is more pronounced in the case of a shot-peening treatment in which a factor of 2 decrease of pit propagation was evidenced [10]. This important result, which has yet to be confirmed in other acidic environments, could be related to a modification of the relaxation kinetics of dislocations during anodic dissolution.

Conclusion

The influence of a pulsed laser-peening treatment on the pitting corrosion behaviour of 316L steel in 0.05 M chloride solution has been investigated. On the basis of rest potentials and characteristic values of potentio-kinetic current density–potential curves, different behaviours have been shown, depending on the kind of LP treatment applied: purely mechanical (M) or thermo-mechanical (TM).

Lower corrosion resistances were observed after the TM treatment due to a severe roughening of the surface, a possible selective ablation of the near-inclusion regions, and a high level of tensile residual stresses at the surface.

Surfaces treated by a mechanical LP exhibited a higher pitting corrosion resistance, with nobler surfaces, and anodic shift of the pit initiation potentials (+0.08 V/SCE), in spite of small roughening effects, and the emergence of planar slip bands. This was attributed to a mechano-electrochemical effect, which could modify the passive film behaviour, and/or the inclusion–matrix interfaces. A modification of the cathodic part of the electrochemical curves (reduction of water and dissolved oxygen around anodic sites), and in turn of the passive behaviour, seems to be the more probable factor to explain observed improvements.

However, a direct correlation between mechanical surface state and electrochemical phenomena is difficult to establish, due to the different scales involved (nm scale for electrochemical phenomena, and μm scale for stress determinations).

References

1. Pan Q, Hang W, Song R, Zhou Y, Zhang G (1998) Surface Coating Technol 102:245
2. Kwok C, Man H, Cheng F (1998) Surface Coating Technol 99:295
3. Clauer AH (1981) In: Shock waves and high strain rate phenomena in metals. Plenum Press, New York, p 675
4. Obata M, Kubo T, Sano Y (2000) Zairyo 49(2):193
5. Peyre P, Scherpereel X, Berthe L, Carboni C, Fabbro R, Beranger G, Lemaitre C (2000) Mater Sci Eng 280(2):294
6. Krauβ M, Herzog R, Scholtes B (2001) Z Metallkd 92(8):910
7. Braham C, Perrais J, Ledion J (1994) 2ème Colloque Européen ''Corrosion Dans Les Usines Chimiques Et Parachimiques''. 206ème Manifestation Fec, Grenoble (Fr)
8. Ben Rhouma A, Braham C, Fitzpatrick ME (2001) J Mater Eng Perf 10:507
9. Ke R, Alkire R (1995) J Electrochem Soc 142(12):4056
10. Carboni C (2002) Doctoral Thesis, University of Technology of Compiègne, Fr
11. Carboni C, Peyre P, Fregonese M, Mazille H (2001) In: Jeandin M, Sudarshan T (eds) Proceedings of surface modifications technologies XIV (Smt14), Paris, Sept. 2000. ASM, p 381
12. Fabbro R, Fournier J, Ballard P, Devaux D, Virmont J (1990) J Appl Phys 68:775
13. Schmidt-Uhlig T (2000) Epj Appl Phys 9(3):235
14. Seo M, Chiba M (2001) Electrochim Acta 47:319
15. Lu J (2005) In: Lu J (ed) Handbook on residual stress measurements, 2nd edn. SEM
16. Gutman EM (1994) Mechanochemistry of solid surfaces, Ed. World Scientific Publishers, Singapore
17. Vignal V, Valot C, Oltra R, Verneau M, Coudreuse L (2002) Corros Sci 44(7):1477
18. Kamachi Mudali U, Katada Y (2001) Electrochim Acta 46:3735